Renewable Energy 43 (2012) 343–353

Contents lists available at SciVerse ScienceDirect

Renewable Energy

journal homepage: www.elsevier.com/locate/renene

Control of a matrix converter for the operation of autonomous systems

Roberto Cárdenas [a,*], Rubén Peña [b], Patrick Wheeler [c], Jon Clare [c], Carlos Juri [a]

[a] Electrical Engineering Department, University of Chile, Avenida Tupper 2007, Postal Code 8370451, Santiago, RM, Chile
[b] Electrical Engineering Department, University of Concepcion, 4074580 Concepción, Chile
[c] Department of Electrical and Electronic Engineering, University of Nottingham, Nottingham University Park, Nottingham NG7 2RD, UK

ARTICLE INFO

Article history:
Received 26 July 2011
Accepted 24 November 2011
Available online 21 December 2011

Keywords:
Distributed generation
Wind-diesel systems
Matrix converters

ABSTRACT

In this paper a new control system for a 4-leg Matrix Converter (MC) feeding an isolated load is discussed. The proposed system is appropriate for wind-diesel schemes or any other application where a path for the circulation of zero sequence currents is required, e.g. wind energy conversion systems feeding isolated loads, small portable diesel generators used in ambulances and similar emergency vehicles, wind hybrid generation systems, wind-diesel schemes, etc. In this work it is assumed that the 4-leg MC is fed from a variable speed diesel-driven Permanent Magnet (PM) generator. A vector control system based in two synchronous rotating *d-q* axes is used to regulate the load voltage. The frames are rotating clockwise and counter-clockwise respectively in order to control the positive and negative sequence of the output signals. A separate resonant controller is used to regulate the homopolar components of the load voltage. The design of the control system is discussed in this work and experimentally validated using a prototype.

1. Introduction

The advantages of variable speed generation are well known [1,2]. Maximum efficiency in the energy conversion process could be achieved by operating the system at an optimal point in the power-speed plane [1–4]. For instance in wind energy conversion systems the maximum steady state aerodynamic efficiency is produced when the power captured by the wind turbine is proportional to the cube of the rotational speed [1]. In diesel engines the maximum Output Power/Fuel consumption ratio is obtained when the rotational speed is changed in order to follow an optimal power-speed curve [3,4].

Variable speed operation of generators has some additional advantages. For instance, reduced mechanical stresses in some components of the systems [1], e.g. gear boxes, blades and less maintenance of diesel generators [3]. When variable speed distributed generation topologies are implemented, improved efficiency is achieved by generating the energy close to the consumption point [5,6]. However, variable speed generation produces electrical signals with fluctuating frequency and voltage magnitudes and power electronics is required in order to feed the load with regulated signals.

A variable speed generation system can be applied in grid-connected or stand-alone generation systems. When the system is feeding a stand-alone load, a neutral connection is required to allow the circulation of zero sequence current components [7,8]. One of the methods to provide a neutral connection is to use a Δ-Y electrical transformer connected to the output of the power converter. Therefore, the neutral point is provided by the star-connected secondary of the electrical transformer. However, in recent publications [8–10], power converters with four output wires have been proposed to feed isolated unbalanced loads. Fig. 1 shows two power converter topologies reported in the literature which can be used to supply electrical energy to isolated single-phase loads [8]. In the schemes shown in Fig. 1, PWM voltage source converters, connected in back-to-back topologies, are used. The machine-side PWM converter could be replaced by a rectifier bridge followed by a step-up chopper [11]. Nevertheless, the Total Harmonic Distortion (THD) in the stator currents is much higher in this case [12].

In the scheme shown in Fig. 1a, the load neutral is tied to a middle-point in the dc-link capacitors. This topology is simple to implement but it is not appropriate when heavily unbalanced loads are fed by the load-side converter [13]. In this case the capacitor ripple current is high and a known drawback of this topology is that excessively large dc-link capacitors could be required. In the

* Corresponding author. Tel.: + 56 2 978 4203; fax: +56 2 6720162.
E-mail addresses: rcd@ieee.org, rcardenas@ing.uchile.cl (R. Cárdenas), rupena@udec.cl (R. Peña), pat.wheeler@nottingham.ac.uk (P. Wheeler), jon.clare@nottingham.ac.uk (J. Clare), Carlos.juri@gmail.com (C. Juri).

0960-1481/$ – see front matter © 2011 Elsevier Ltd. All rights reserved.
doi:10.1016/j.renene.2011.11.052

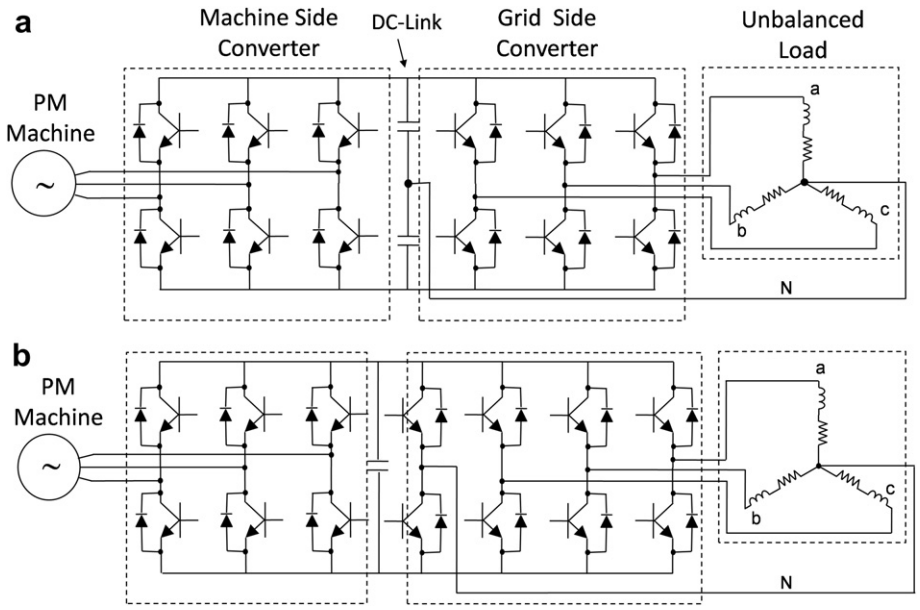

Fig. 1. Two topologies, based in back-to-back PWM voltage source converters, currently used to allow the circulation of zero sequence currents in the isolated load. a). The load neutral is tied to a mid-point of the dc-link capacitors. b) The neutral point is provided by a 4-leg converter at the load-side.

topology shown in Fig. 1b, the neutral point is provided by an additional leg implemented with two semiconductor switches [8]. Using the adequate modulation algorithm, for instance a three-dimensional Space Vector Modulation (SVM) algorithm [14], the line to neutral output voltages v_{an}, v_{bn}, v_{cn} are synthesised and independently controlled.

A topology similar to that shown in Fig. 1b is obtained when the back-to-back 3 × 4 PWM voltage source inverter is replaced by a 3 × 4 MC. This topology provides bidirectional power flow, sinusoidal input/output currents and controllable input displacement factor [15–17]. When compared to back-to-back converters, the MC has some significant advantages. For instance, due to the absence of electrolytic capacitors, the MC can be more robust and reliable. The space saved by an MC, compared to a conventional back-to-back converter, has been estimated as a factor of three [16]. Because of the good power to size ratio, 4-leg MCs can be used in portable generacion systems, for instance in variable speed diesel generation [10], variable speed wind-diesel topologies, distributed generation applications, emergency vehicles [18], etc.

A topology considering a 4-leg matrix converter, replacing the back-to-back converter, is shown in Fig. 2. The PM generator is feeding the matrix converter input. A second order filter reduces the THD of the input current. Typically a resistor is connected in parallel with the filter inductance to increase the input-stage damping coefficient [19]. Twelve bidirectional switches are required in the 3 × 4 MC to connect the three input terminals to the four outputs. In this paper, the control systems required to regulate the load voltages are analysed and extensively discussed.

The rest of this paper is organised as follow. In Section 2 the proposed control system is extensively discussed. In Section 3 variable speed diesel generation systems are briefly discussed. In Section 4 experimental results are analysed. Finally an appraisal of the proposed control system is presented in the conclusions.

2. Proposed control system

Control systems based on synchronously rotating reference frames are a standard method for the regulation of voltages and currents in electrical machines and power converters. Using *d-q* rotating frames, 3Φ voltages and currents are transformed into dc signals for steady state operation. After the signals are referred to the *d-q* frame, the design of the control loops is straightforward and the required closed loop bandwidth is usually achieved with simple compensators (in most cases PI controllers are sufficient to obtain good dynamic response in the whole operating range).

A conventional *d-q* control system for 4-leg MCs was discussed in [10]. However this control system does not consider the regulation of the negative and zero sequence component of the MC output signals. Therefore this methodology is not appropriate for voltage control when heavily unbalanced loads are fed by the 4-leg MC.

A Resonant Control (RC) system has been proposed in [7,20] for 4-leg power converters. Resonant controllers have some

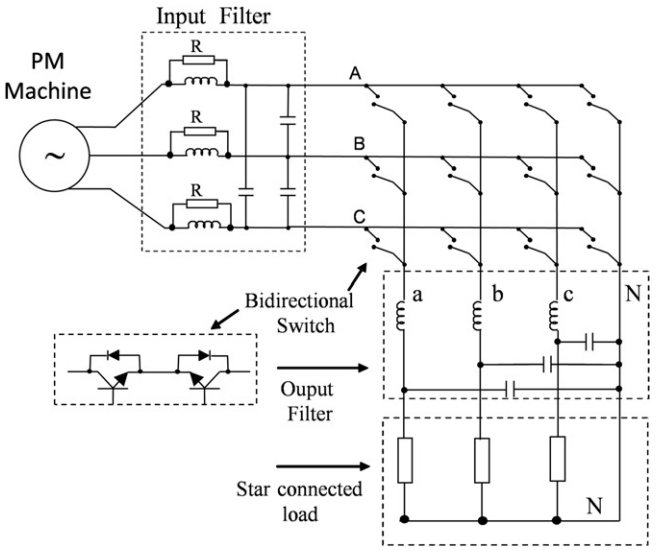

Fig. 2. A topology approximately equivalent to that shown in Fig. 1b implemented considering a 4-leg matrix converter.

advantages and disadvantages when compared to *d-q* based controllers. For instance a single RC per phase can be used to regulate the positive, negative and zero sequence components of the line to neutral load voltage. However, for the control of linear unbalanced loads, the *d-q* system is more flexible because is relatively simple to design controllers with different closed loop poles for each sequence. This is an advantage in systems where the negative and zero sequence impedances are not equal to the positive sequence impedance [21] [22]. An additional advantage of a *d-q* control system is obtained when the plant is fully decoupled (i.e. no interaction between the *d* and *q* axis is produced). In this case the same controller produces identical dynamic response irrespective of the operating frequency. In this case only the controller regulating the zero sequence component has to be adjusted in order to eliminate the variable frequency homopolar signals. Additionally, as stated before, it is relatively simple to design controllers, with good dynamic response, in *d-q* rotating frames.

In this paper, the application of *d-q*-0 controllers, composed of *d-q* controllers to regulate the positive/negative sequence load voltage, and a resonant controller to regulate the zero sequence load voltage are discussed.

2.1. Symmetrical components

Assuming that the cross-coupling between the *d* and *q* axis are compensated considering decoupling terms at the controller outputs (see Section 2.3), the transfer function between the MC line to neutral output voltage of phase *a*, and the corresponding load voltages is:

$$G_a(s) = \frac{V_{aL}}{VaN} = \frac{R_{La}}{s^2 R_{La} C_f L_f + sL_f + R_{La}} \tag{1}$$

The transfer functions $G_b(s)$ and $G_c(s)$ are obtained by replacing R_{La} with R_{Lb} and R_{Lc} respectively. Because of simplicity, a resistive load is considered in (1). However the control systems discussed in this work could be modified to regulate the voltages of loads with inductive and capacitive power factors.

Fortescue in 1918 presented the concept of symmetrical components [23]. As stated in his work, an unbalanced 3Φ system can be represented as three balanced systems of positive negative and zero sequence signals as:

$$\begin{bmatrix} V_{aL} \\ V_{bL} \\ V_{cL} \end{bmatrix} = \begin{bmatrix} V_{aL0} & V_{aL}^{+} & V_{aL}^{-} \\ V_{bL0} & V_{bL}^{+} & V_{bL}^{-} \\ V_{cL0} & V_{cL}^{+} & V_{cL}^{-} \end{bmatrix} \tag{2}$$

where the super-scripts "+" and "−" stand for positive and negative sequences respectively. The sub-script "0" stands for the zero sequence components. As shown in Fig. 3, the sequence components can be represented as a system rotating counter-clockwise, another system rotating clockwise and the three homopolar components which are of the same magnitude and phase. The symmetrical components can be obtained as:

$$\begin{bmatrix} V_{aL0} \\ V_{aL}^{+} \\ V_{aL}^{-} \end{bmatrix} = \frac{1}{3}\begin{bmatrix} 1 & 1 & 1 \\ 1 & a & a^2 \\ 1 & a^2 & a \end{bmatrix}\begin{bmatrix} V_{aL} \\ V_{bL} \\ V_{cL} \end{bmatrix} \rightarrow [V]_{+-0} = [T][V]_{abc} \tag{3}$$

Where $a = e^{j2\pi/3}$. Using (1), the load voltage can be written as:

$$\begin{bmatrix} V_{aL} \\ V_{bL} \\ V_{cL} \end{bmatrix} = \begin{bmatrix} G_a(s) & 0 & 0 \\ 0 & G_b(s) & 0 \\ 0 & 0 & G_c(s) \end{bmatrix}\begin{bmatrix} V_{aN} \\ V_{bN} \\ V_{cN} \end{bmatrix} \tag{4}$$

In steady state, assuming $s = j\omega_o$ (Fourier representation) and using (3) in (4), balanced operation of the load voltage is obtained when:

$$\begin{bmatrix} V_{aN0} \\ V_{aN}^{+} \\ V_{aN}^{-} \end{bmatrix} = [T]\begin{bmatrix} G_a(j\omega_o) & 0 & 0 \\ 0 & G_b(j\omega_o) & 0 \\ 0 & 0 & G_c(j\omega_o) \end{bmatrix}^{-1}[T]^{-1}\begin{bmatrix} 0 \\ V_{aL}^{+} \\ 0 \end{bmatrix} \tag{5}$$

where V_{aN0}, V_{aN}^{+} and V_{aN}^{-} are the zero, positive and negative sequence components of the MC output voltage respectively. Equation (5) shows that it is possible to synthesise a balanced load voltage even when $G_a(j\omega_o) \neq G_b(j\omega_o) \neq G_c(j\omega_o)$. However, because the transfer functions $G(j\omega_o)$ are load dependant, a control system is required to regulate the 4-leg MC output, compensating for the load changes.

2.2. Control systems based on counter-rotating reference frames

The control system proposed in this work is shown in Fig. 4. The matrix converter is connected to the unbalanced load through a second order power filter. The MC output currents are measured using Hall-effect transducers. These currents are required for the 4-step commutation method and to implement the overcurrent protection system. Three Hall-effect voltage transducers are connected to the MC output, for measuring the load voltage. Additionally, two voltage transducers are used to measure the input voltage which is required in the SVM algorithm. The SVM algorithm used in this work is presented in [14].

When an unbalanced load is connected to the MC output, the voltages and currents can be referred to two rotating axes, rotating clockwise and counter-clockwise respectively [22]. This is shown in Fig. 5. The angle of the positive sequence *d-q* axis respect to the stationary frame is θ_e^{+}, and that of the negative sequence *d-q* axis is θ_e^{-}. The load voltage vector, referred to these axes, is obtained as:

$$v_{dL}^{+} = v_{\alpha L}\cos\left(\theta_e^{+}\right) + v_{\beta L}\sin\left(\theta_e^{+}\right) \tag{6}$$

$$v_{qL}^{+} = -v_{\alpha L}\sin\left(\theta_e^{+}\right) + v_{\beta L}\cos\left(\theta_e^{+}\right) \tag{7}$$

$$v_{dL}^{-} = v_{\alpha L}\cos\left(\theta_e^{-}\right) + v_{\beta L}\sin\left(\theta_e^{-}\right) \tag{8}$$

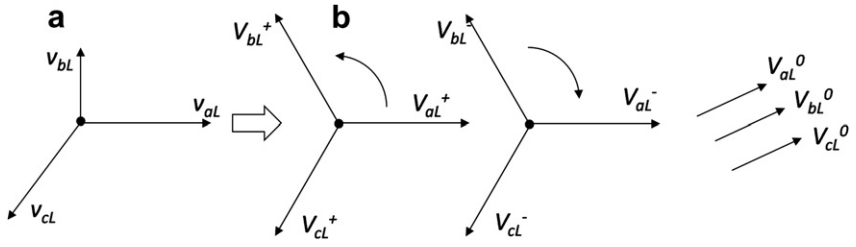

Fig. 3. Fortescue decomposition. a) Unbalanced system. b) Equivalent systems with positive, negative and zero sequence components obtained using the matrix *T* defined in (3).

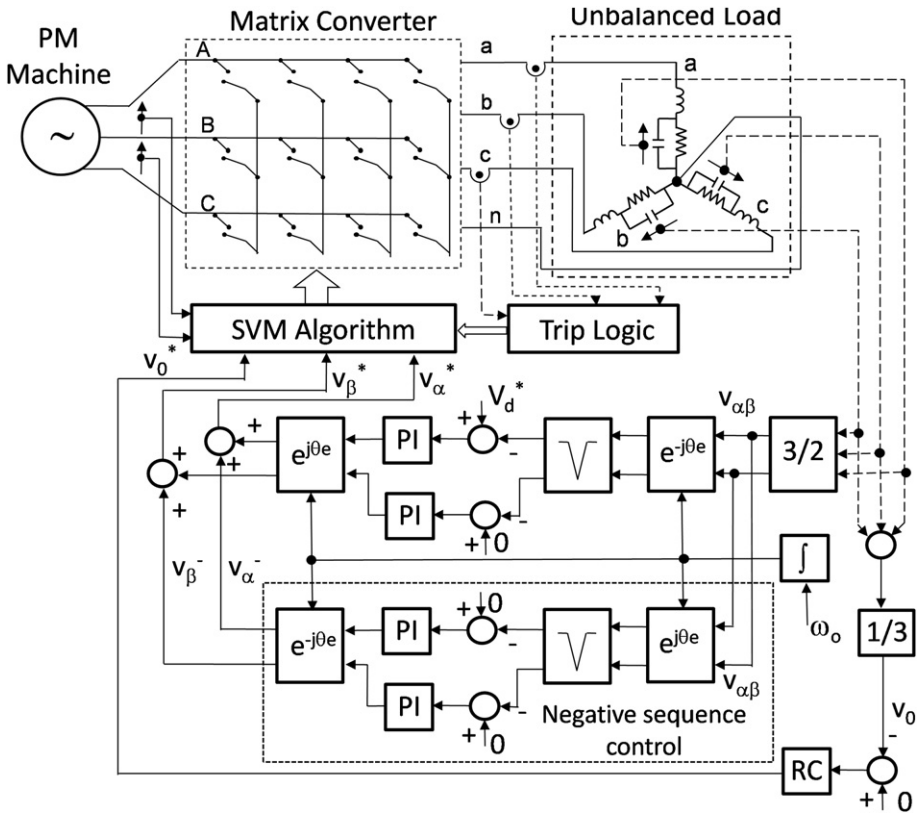

Fig. 4. Control system proposed in this work.

$$v_{qL}^{-} = -v_{\alpha L}\sin\left(\theta_e^{-}\right) + v_{\beta L}\cos\left(\theta_e^{-}\right) \tag{9}$$

where $v_{\alpha L}$, $v_{\beta L}$ are the α-β components of the load voltage. The angles θ_e^+ and θ_e^- are the angles of the axes rotating counter-clockwise and clockwise respectively. Both angles are measured with respect to the stationary frame. In this work it is assumed that $\theta_e^- = -\theta_e^+$ and $\theta_e^+ = \theta_e$ (see Fig. 4).

As it is well known, negative sequence voltages produce a double frequency signal in the positive sequence synchronous rotating frame [24]. This double frequency signal might be eliminated using a notch filter (see Fig. 4). In the Laplace domain this is written as:

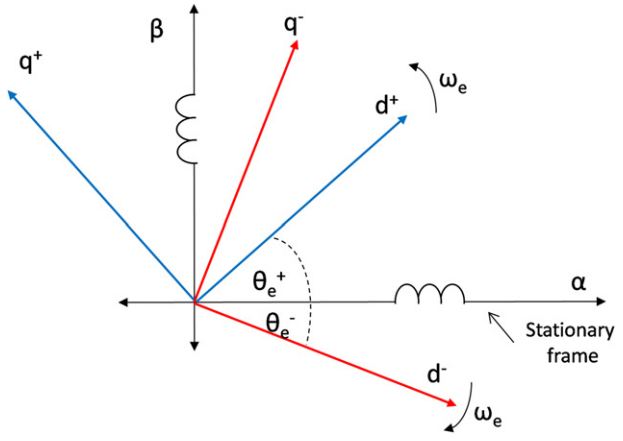

Fig. 5. The two counter-revolving synchronous rotating axes.

$$v_{dLf}^{+}(s) + jv_{qLf}^{+}(s) = \left[v_{dL}^{+}(s) + jv_{qL}^{+}(s)\right]\frac{s^2 + 4\omega_o^2}{\left(s^2 + 4\zeta\omega_o s + 4\omega_o^2\right)} \tag{10}$$

where ω_o is the output frequency. Using the same methodology, the double frequency signal produced (by the positive sequence voltage) in the negative sequence rotating frame could be eliminated using [22]:

$$v_{dLf}^{-}(s) + jv_{qLf}^{-}(s) = \left[v_{dL}^{-}(s) + jv_{qL}^{-}(s)\right]\frac{s^2 + 4\omega_o^2}{\left(s^2 + 4\zeta\omega_o s + 4\omega_o^2\right)} \tag{11}$$

Using (6)–(11) the control system shown in Fig. 4 could be implemented. When two revolving axes are considered, the *d-q* notch-filtered load voltages can be independently regulated. As shown in Fig. 4, the references for the negative sequence *d-q* voltage and the positive sequence quadrature voltage, are set to zero.

2.3. Control system design for the regulation of the positive and negative sequence components of the load voltage

A simplified block diagram of the control system is shown in Fig. 6. The plant is represented in α-β coordinates. Because of the notch filters, it is assumed that there is a negligible coupling between the positive and negative sequence in the control system. To design the controllers the plant has to be referred from α-β to *d-q* coordinates In this work the frequency shifting property of the Laplace transform is used [25], instead of the time based approach presented previously in [26,27].

In Fig. 6 an *m*th order plant is assumed, with a transfer function N(*s*)/D(s), with $N(s) = s^n + a^{n-1}s^{n-1} + a^{n-2}s^{n-2} + \ldots a_0$. Similarly,

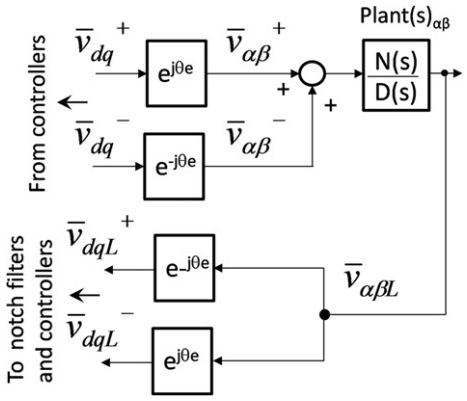

Fig. 6. Simplified block diagram used to refer the plant dynamic to d–q coordinates.

the denominator can be written as $D(s) = s^m + b_{m-1}\, s^{m-1} + b_{m-2}\, s^{m-2} + \ldots b_0$. Therefore, using superposition the dynamic of the system for the positive sequence signals is:

$$\frac{d^n\left(\bar{v}_{dq}^{+}e^{j\theta e}\right)}{dt^n} + a_{n-1}\frac{d^{n-1}\left(\bar{v}_{dq}^{+}e^{j\theta e}\right)}{dt^{n-1}} + \cdots a_0\left(\bar{v}_{dq}^{+}e^{j\theta e}\right) = \frac{d^m\left(\bar{v}_{dqL}^{+}e^{j\theta e}\right)}{dt^n} + b_{m-1}\frac{d^{m-1}\left(\bar{v}_{dqL}^{+}e^{j\theta e}\right)}{dt^{m-1}} + \cdots b_0\left(\bar{v}_{dqL}^{+}e^{j\theta e}\right) \quad (12)$$

The frequency shifting property of the Laplace transform is represented by:

$$\mathcal{L}\left(f(t)e^{-j\omega_e t}\right) = F(s+j\omega_e) \quad (13)$$

where the symbol "$\mathcal{L}$" represents the Laplace transform. Assuming that $\omega_e = d\theta/dt$ and restricting the order of (12) to $m = 2$ and $n = 2$, without loss of generality, then (12) in the Laplace domain can be written as:

$$\left[(s+j\omega_e)^2 + a_1(s+j\omega_e) + a_0\right]\bar{v}_{dq}^{+} = \left[(s+j\omega_e)^2 + b_1(s+j\omega_e) + b_0\right]\bar{v}_{dqL}^{+} \quad (14)$$

Using (13) and (14) the plant in the stationary frame can be referred to the positive synchronous rotating frame and vice versa. Therefore, the transfer function of (1) can be referred to the positive sequence rotating frame as:

$$G_{dq}(s) = \frac{\bar{v}_{dqL}^{+}(s)}{\bar{v}_{dq}^{+}(s)} = \frac{R_{La}}{(s+j\omega_e)^2 R_{La}C_f L_f + (s+j\omega_e)L_f + R_{La}} = \frac{R_{La}}{s^2 C_f L_f R_{La} + \left(L_f + 2jL_f C_f R_{La}\omega_e\right)s + \left(j\omega_e L_f + R_{La} - C_f L_f R_{La}\omega_e^2\right)} \quad (15)$$

In d-q control systems, decoupling terms are usually added to the controller output in order to eliminate the coupling between the d-q axis in the transfer function of (15) (see Fig. 7). These terms usually increase the bandwidth of the closed loop control system and are considered important in systems where high dynamic response is required [28,29].

The transfer function for the decoupling terms is plant dependent. The transfer function $DT^{+}(s)$ is calculated using $G_{dq}(s)$ (see (15)) and (1) as:

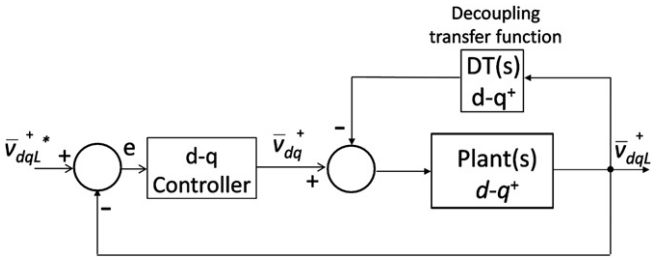

Fig. 7. Control system in d–q coordinates and including decoupling terms.

$$\frac{G_{dq}(s)}{1 + G_{dq}(s)DT^{+}(s)} = G(s) = \frac{R_L}{s^2 R_L C_f L_f + sL_f + R_L} \quad (16)$$

Using (16) $DT^{+}(s)$ can be calculated as:

$$DT^{+}(s) = \left(2jC_f L_f \omega_e s + jL_f\omega_e/R_a - C_f L_f \omega_e^2\right)\bar{v}_{dqL}^{+} \quad (17)$$

Because of the difficulties associated with the implementation of a real time differentiation, the decoupling terms can be approximated as:

$$DT^{+}(s) \approx \left(jL_f\omega_e/R_a - C_f L_f \omega_e^2\right)\bar{v}_{dqL}^{+}(s) \quad (18)$$

After some manipulation it is relatively simple to demonstrate that (18) can be simplified to:

$$DT^{+}(s) \approx j\omega_e L_f i_{dq}^{+}(s) \quad (19)$$

Where $\bar{\imath}_{dq}^{+}$ is the MC output current referred to the positive sequence d-q frame. In a 4-leg matrix converter the four output currents (i_a, i_b, i_c and i_n) are usually measured, because they are required in the modulation algorithm to implement the 4-step commutation method [15,17].

Using a methodology similar to that depicted in (14)–(19), and using $\mathcal{L}(f(t)e^{j\omega_e t}) = F(s - j\omega_e)$, it could be demonstrated that the compensation terms for the negative sequence control system are approximated by:

$$DT^{-}(s) \approx j\omega_e L_f \bar{i}_{dq}^{-}(s) \quad (20)$$

The frequency response of the positive sequence transfer function $\bar{v}_{dqL}(s)/\bar{v}_{dqL}^{*}(s)$ (see Fig. 7) is shown in Fig. 8. For this graphic the d-q controllers have been designed for a phase margin of 65° and a bandwidth of about 80 Hz. For the plant the values of $R_L = 10\ \Omega$, $C_f = 40\ \mu F$ and $L_f = 4$ mH have been considered. As shown in Fig. 8b, the shape of the Bode response is significantly changed when the decoupling terms of (19) are not considered and this affects the bandwidth but also the phase margin of the open loop transfer function. This has already been mentioned in [28,29].

Using the decoupling terms in the control structure of Fig. 4, the positive and negative sequence controllers could be designed considering a plant dynamic similar to that obtained in α-β coordinates. In this case standard linear tools as for instance root locus

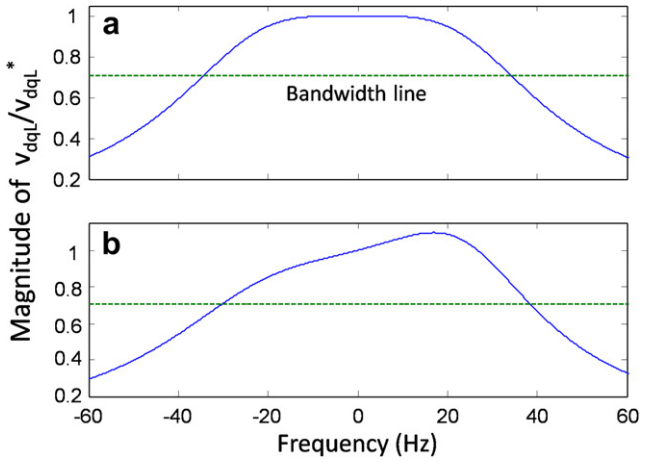

Fig. 8. Bode plot showing the magnitude v^{+}_{dqL}/v^{+*}_{dqL}. a) Considering the decoupling terms. b) Without considering the decoupling terms.

could be used for design purposes. This is shown in Fig. 9 where a digital controller is designed in the z-plane using root locus, in order to regulate the positive sequence load voltage. For this case, for the output filter the values of $C_f = 40$ μF and $L_f = 4$ mH have been considered. A delay of one sample time is considered to represent the SVM algorithm. To consider the worst case situation, the controller is designed when the output is feeding the second order power filter only; therefore the output stage is operating with almost zero damping (no resistive load is connected to the output). A lead-lag network is added to the PI controller in order to obtain damping coefficient above 0.6 for all the dominant closed loop poles.

2.4. Control system to regulate the zero sequence load voltage

The homopolar components are not reflected in the rotating *d-q* frames (they are eliminated by the α-β transformation). Therefore the zero sequence voltage cannot be controlled using the rotating frames shown in Fig. 4. In this work it is proposed to regulate the homopolar components of the load voltage using a control system implemented in the stationary frame.

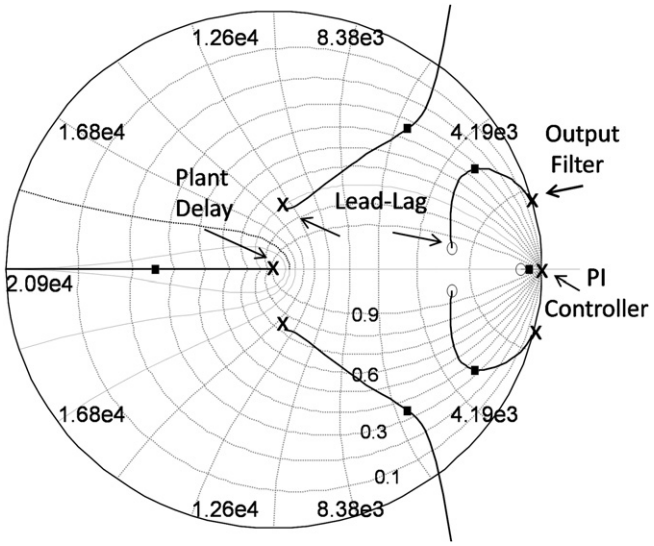

Fig. 9. Root locus for the design of the positive sequence PI controller.

Because the zero sequence voltage is sinusoidal, standard PI controllers cannot regulate this component with zero steady state error. Therefore, resonant controllers are proposed in this application. A single resonant controller, as the one labelled "RC" in Fig. 4 might be used to drive the zero sequence error to zero.

In the Laplace plane an RC is composed of a couple of purely imaginary poles with a resonant frequency of ω_o, where ω_o is the desired output frequency. In the *s*-plane, a typical resonant controller has the transfer function [30,31]:

$$G_c(s) = K_c \frac{s^2 + 2\zeta\omega_n s + \omega_n^2}{s^2 + \omega_o^2} \tag{21}$$

where K_c is the controller gain. In the numerator of (21), zeros located close to the resonant poles, might be used to improve the dynamic response. In the *z*-plane, the transfer function of the resonant controller is [7]:

$$G_c(z) = K_{cz} \frac{z^2 + a_1 z + a_2}{z^2 + b_1 z + b_2} \tag{22}$$

In this case the resonant poles are located along the unit circle instead of the $j\omega$ axis (as in the case of the "*s*" implementation of (21)). In the frequency domain, the tracking error $e(j\omega)$ is calculated as:

$$e(j\omega_o) = \frac{V^*_{aL}(j\omega_o)}{1 + G_c(j\omega_o)\mathrm{SVM}(j\omega_o)\mathrm{Plant}(j\omega_o)} \tag{23}$$

The operating principle of the RC is that $|G_c(j\omega)| \to \infty$ for a frequency $\omega = \omega_o$ (see (23)). Therefore the error calculated from (23) is zero for a sinusoidal reference voltage (V^*_{aL}) of frequency ω_o.

The resonant controller proposed in this work has to be designed considering the zero sequence plant. The reference signal for the zero sequence control system is set to zero. More information about resonant controllers is elsewhere [7,28,30].

3. Variable speed diesel generation

Most diesel generation systems operate at constant rotational speed due to the restriction of constant frequency at the generator terminals. However, for light loads and rated speed operation, not all the fuel is burned by the engine and this increases maintenance costs [3,4,18]. Additionally, diesel engines have high fuel consumption when operating at light and constant speed. In some diesel generation systems a minimum load of about 40% is usually recommended by the manufacturers [4].

To avoid this problem, the operation of variable speed diesel engines have been reported in the literature. The main advantage of

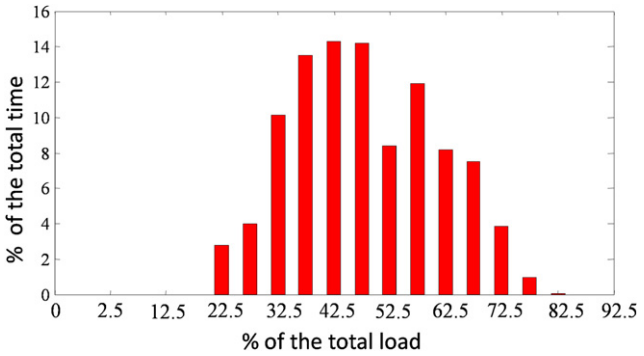

Fig. 10. Frequency distribution for a typical October (Spring season in the southern hemisphere). The load is measured at "*Villa Tehuelche*", a small village in the Chilean Patagonia.

variable speed operation is that the fuel consumption can be substantially reduced. Moreover, the engine life is increased because the diesel engine is run at low speed for light load, reducing the overall thermal signature [18].

The advantages of variable speed generation can be further explained using the load profile of a small rural village. In Fig. 10 the electrical load characteristics measured during October at "*Villa Tehuelche*", a small village in Chilean Patagonia is shown. A fixed speed diesel system is used to supply electricity to the village, during part of the day (typically from 6:30 AM to ≈12:000 PM), the nominal power of the diesel engine is about 115 kW, feeding approximately 35–40 households. During spring and summer, most of the time the load is below 50% of the nominal value. The maximum load may occur few times during the year, probably in winter because electric heating is required by the village inhabitants.

The load variation is not only dependant on the season of the year. During day time there are also important fluctuations. This is shown in Fig. 11. Fig. 11a shows the load variation on Sunday, and Fig. 11b, shows the load profile for a Monday in mid September. Considering the information depicted in Figs. 10 and 11 it is concluded that the diesel generator is operating with light loads during a substantial part of the time. Considering the typical low efficiency of a diesel generator operating at light load nominal speed [18], the operation of the system could be optimised if variable speed operation of the engine is allowed. Moreover, if a wind-variable speed diesel system is considered, further maximisation of the fuel saving could be achieved.

Fig. 12a shows the fuel consumption curves obtained experimentally (in a project led by the authors) for a 3 kW, 220 V, 50 Hz diesel engine, for six rotational speeds. According to Fig. 12, at 1 kW, there is ≈90% of additional fuel consumption when the system is operated at 1300 rpm instead of 700 rpm. Fuel efficiency also decreases when the power supplied by the DGS is increased without increasing the rotational speed. Therefore any increase/decrease in load power should be accompanied by and increase/decrease in the rotational speed to improve the system efficiency. From the fuel consumption characteristic of Fig. 12a, a continuous function for the optimal curve in the power-rotational speed plane for minimum fuel consumption can be obtained. This is shown in Fig. 12b.

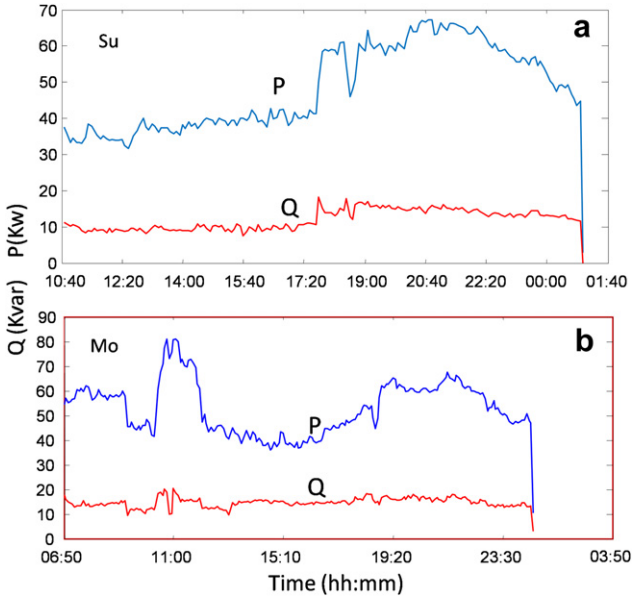

Fig. 11. Load characteristic measured in ("*Villa Tehuelche*"). a) Sunday 17th of September. b) Monday 18th of September.

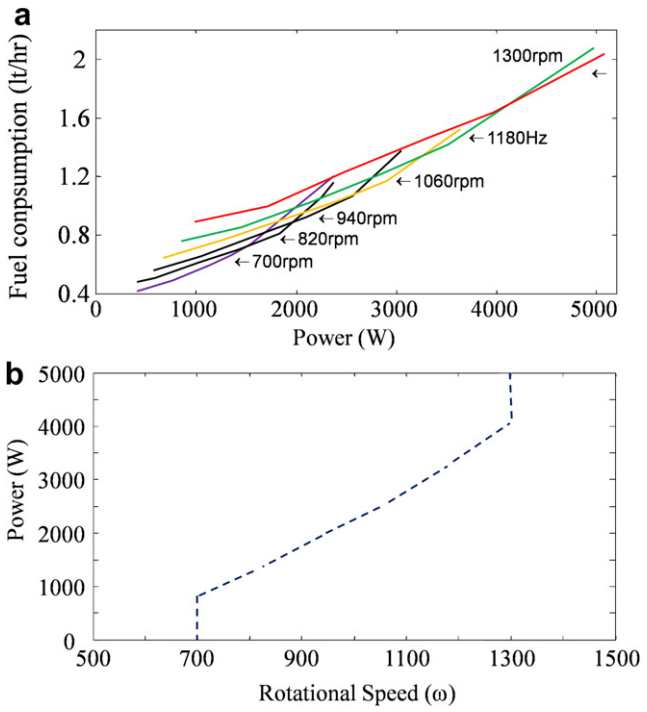

Fig. 12. Experimental tests for a 3 kW, 1000 rpm diesel engine. a) Fuel consumption vs. power for several rotational speeds. b) optimal speed power curve.

4. Experimental results

The control system of Fig. 4 was implemented in the 2.5 kW experimental rig of Fig. 13. The SVM algorithm and proposed control systems are implemented using a DSP based control board and an FPGA, the latter implementing the four-step commutation method [17] and providing the switching signals for the IGBT gate drivers. The DSP board used in this application is a high performance TI TMS320C6713, capable of a peak performance of 1350MFLOPS. For data acquisition purposes two external boards, with a total of 20 Analogue to Digital (ADC) channels of 14 bits, 1 μs conversion time each, are interfaced to the DSP. There are 4 Digital to Analogue (DAC) channels available in these boards. Hall-effect transducers are used to measure the input currents, input voltages and output currents. Anti-aliasing filters are applied to the signals before being sampled by the ADCs.

For the experimental tests involving frequency and voltage variations at the MC input, a 5 kW, 2000 rpm Permanent Magnet Generator (PMG) is connected to the 4-leg MC input. A commercial inverter and a speed-controlled cage machine are used to drive the PMG. In order to emulate a small diesel engine, the methodology reported in [1,4] is used. The non-linear model of the diesel engine used in this work, is reported in [4,32].

The emulation of the diesel engine or any other prime mover (for instance a wind turbine) is controlled by sending a speed reference signal to the commercial inverter. A high resolution position encoder of 10.000 pulses per revolution is used to measure the generator speed. At the matrix converter output a star-connected three-phase load and a second order power filter are connected. This output filter is used to reduce the harmonic content in the voltages and currents. Unless otherwise stated, the sampling time used by the SVM and control algorithm is 100 μs. In the appendix, additional parameters of the experimental system are presented.

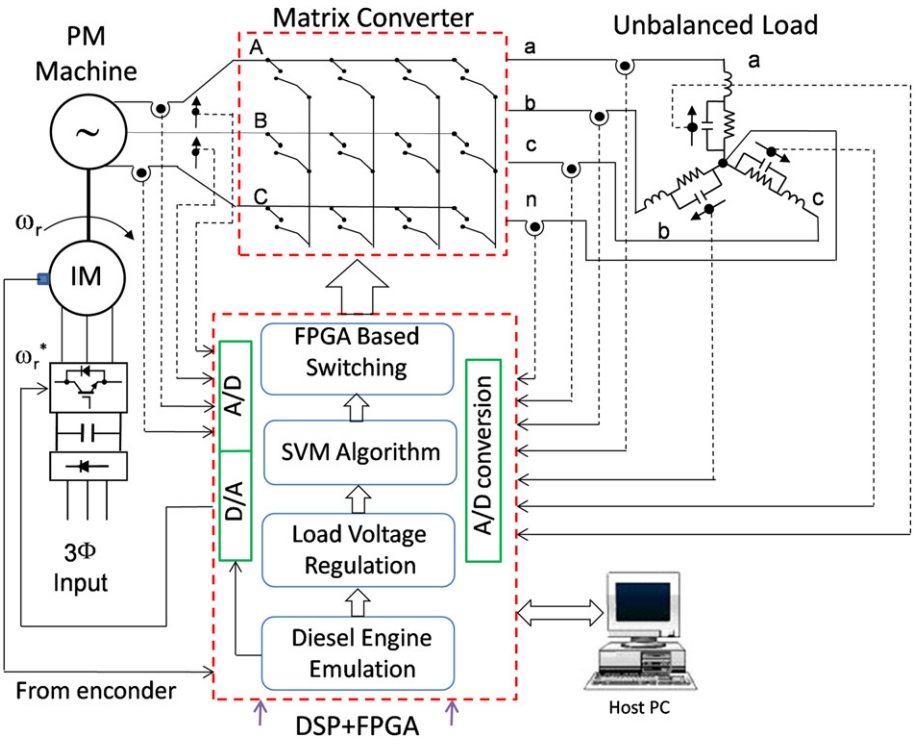

Fig. 13. Experimental system.

In Fig. 14, the load voltages for open loop operation of the proposed generation system are shown. The system is operating in steady state with a load current of 4 A (peak), when a load step is applied to phase *c*, producing a noticeable reduction in the voltage of that phase (see Fig. 14a). In Fig. 14b, the waveform corresponding to $V_{aL}+V_{bL}+V_{cL}$ is depicted. As shown in this graphic, for open loop operation, there is a relatively large zero sequence voltage at the load, after the unbalanced step is applied.

In Figs. 15 and 16, the performance of the *d*-*q*-0 control system, corresponding to a load step identical to that discussed previously, is shown. The load step increases the current in phase *c* to 8 A. In Fig. 14b the MC neutral current is depicted which increases from 0 A to 4 A due to the unbalance. In Fig. 14c the load voltages are shown. Despite the relatively large variation in phase *c*, the control system regulates the voltages with little variations. The negative and zero sequence components of the regulated signals have been virtually eliminated.

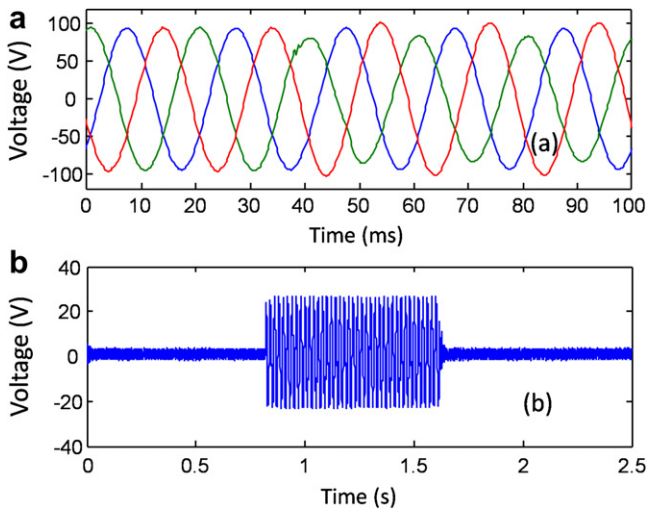

Fig. 14. Open loop performance for an unbalanced load step in phase *c*. a) Load voltages. b) Zero sequence components of the load voltage.

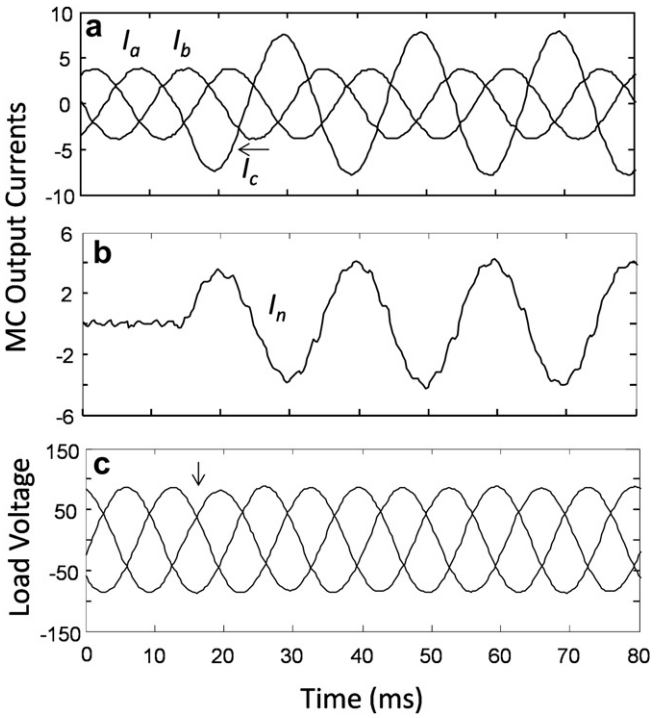

Fig. 15. Performance of the control system for a load step in phase c. a) Currents I_a, I_b and I_c measured at the matrix converter output. b) Neutral current c) Phase to neutral load voltages.

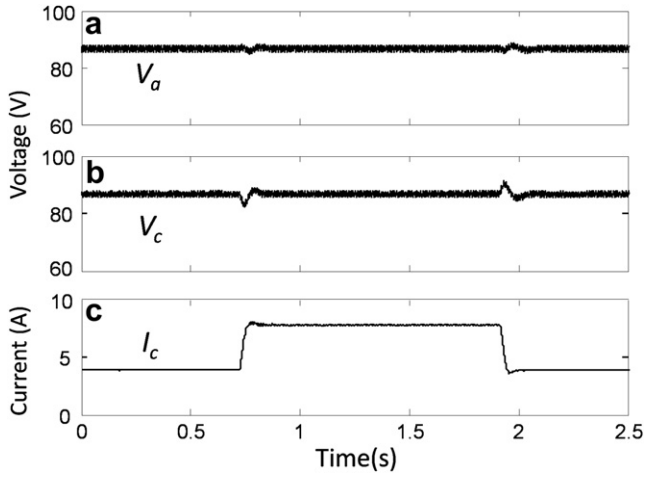

Fig. 16. Performance of the control system for a load connection/disconnection in phase c. a) Voltage in phase a. b) Voltage in phase c. c) MC output current in phase c.

In Fig. 16 a similar test, but shown in a different timescale, is shown. In this case the load step is applied to phase c in $t \approx 1.75$ s and disconnected in $t \approx 1.9$. Fig. 16a and b show the voltage variations in phases a and c respectively (the modulus of the signal is shown instead of the instantaneous values). As shown in these graphics the voltage dip and overshoot are relatively small despite the unbalanced load step applied to phase c (see Fig. 16c). The waveform corresponding to the voltage in phase b is similar to that shown in Fig. 16a.

The response of the proposed generation system has been tested for variable speed operation of the PM generator. This is shown in Figs. 17 and 18. In Fig. 17a the rotational speed of the PM generator is depicted. The system is operating between $\approx$1100 rpm and $\approx$1800 rpm. As expected, the phase to neutral input voltage has identical waveform shape to the rotational speed (see Fig. 17c). In Fig. 17b the input current is shown. Because the load power is constant, the input current is proportional to $1/V_{in}$ (or $1/\omega_r$), as shown in Fig. 17b.

Fig. 18 shows the voltage transfer ratio, defined as V_{out}/V_{in} (V_{out} is the MC output voltage) and the phase to neutral load voltage. As shown in Fig. 18a, the voltage transfer ratio is also proportional to $1/V_{in}$ with a similar waveform shape to that of the MC input current. Fig. 18b shows the load voltage, which is well regulated despite the fast changes in the PM rotational speed.

The performance of the system considering a load step during a fast ramp speed variation is shown in Fig. 19. The speed is changed

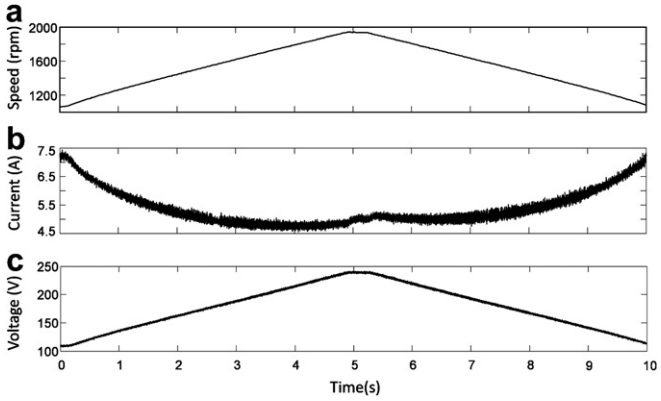

Fig. 17. Variable speed operation of the system. a) Rotational speed. b) MC input current. c)MC input phase to neutral voltage.

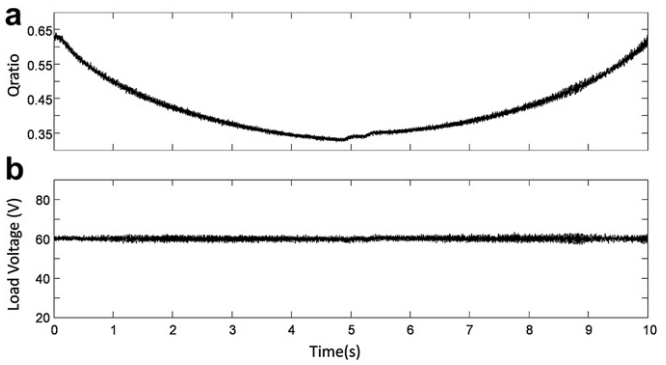

Fig. 18. Control system response considering the test of Fig. 17. a) Voltage transfer ratio. b) Load voltage.

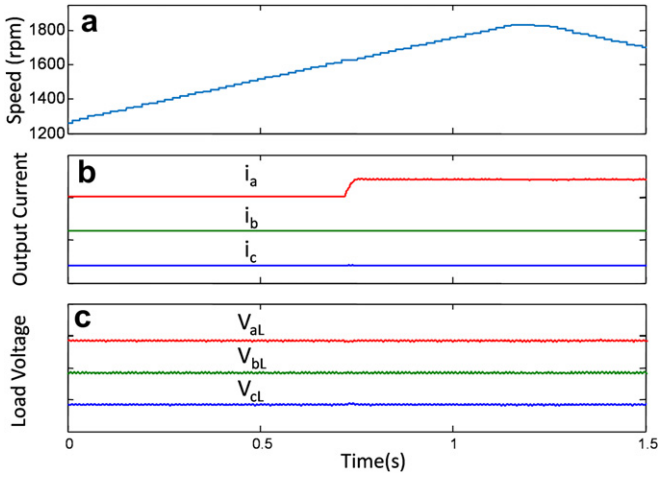

Fig. 19. Load step variation produced during a ramp speed change. a) Rotational speed. b) MC output current. c) Load voltages.

from 1200 rpm to 1800 rpm in 1.25 s. In $t \approx 0.7$ s a load step is applied to phase a as shown in Fig. 19b. Before the step the MC output current is about 3 A for all the phases. After the load step the current in phase a is increased to about 6 A.

The load voltages are shown in Fig. 19c. Each phase to neutral voltage is adjusted at 80 V. When the voltage step is applied the voltage variations are negligible, showing that for even fast speed variations the control system is able to maintain the voltage well regulated.

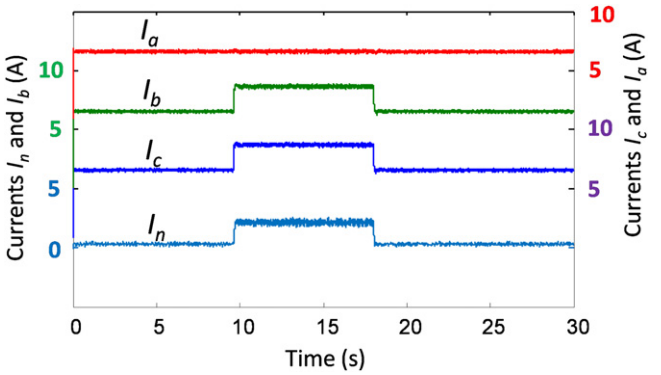

Fig. 20. Phase and neutral currents at the MC output, considering load step variations in two of the phases and variable speed diesel emulation.

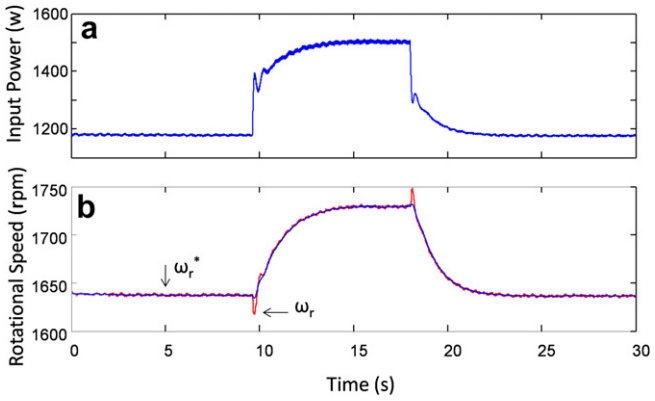

Fig. 21. Control system response corresponding to the test of Fig. 20. a) Input power, b) Rotational speed.

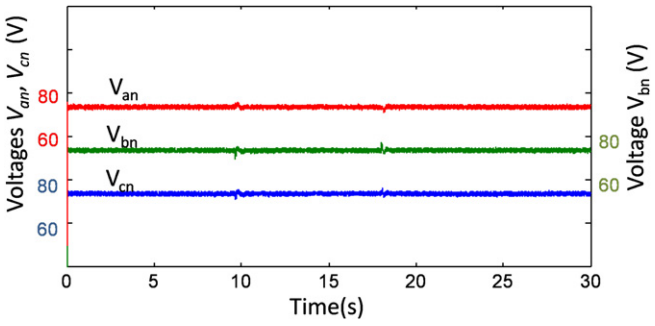

Fig. 22. Voltage system response corresponding to the test of Fig. 20.

The performance of the system considering variable speed diesel generation is shown in Figs. 20–22. A variable speed diesel generator of 3 kW is emulated using the hardware-in-the-loop methodology reported in [4]. An optimum power-speed curve, similar to that shown in Fig. 12b, is stored in a look-up table and used to determine the operating speed of the diesel engine. The system is operating at about 1650 rpm when load step variations are applied in two of the phases respect to the neutral point. This is shown in Fig. 20 where the variation in the MC output currents is depicted, including the neutral current which is increased to compensate for the unbalance. Fig. 21a shows the average active power. This value is measured at the PM generator terminals using Hall-effect transducers. A second order filter is used to obtain the low frequency component of the power which is shown in Fig. 21a.

Fig. 21b shows the rotational speed. After the load step, the speed of the emulated diesel engine is increased to a new operating point to minimise the fuel consumption. When the load is disconnected, the engine is again moved to the previous operating point.

Fig. 22 shows the load voltage waveform. Despite the load steps and the variation in the input voltage and frequency produced at the MC input, the load voltage is well regulated with a small dip and overshoot produced when the load variation is applied to the generation system.

5. Conclusions

In this work, a control system composed of *d-q* controllers implemented in counter-rotating synchronous frames, to regulate the positive and negative components of the load voltage has been presented. The *d-q* control system is augmented with a resonant controller which is designed to eliminate the homopolar voltage components from the load.

The control system has been tested for highly unbalanced linear loads, considering fixed and variable speed operation of the PM generator connected at the MC input. The performance obtained is considered appropriate.

The behaviour of the proposed generation system, considering unbalanced load steps and the emulation of variable speed diesel engines have been investigated in this work. In all the cases the control system response have been appropriate with a good settling time and dynamic performance. The control system proposed in this work is not computationally intensive and can be implemented in a DSP platform operating with a relatively high sampling frequency. Therefore the switching frequency is also relatively high and the size of the input/ouput filters can be reduced.

Acknowledgements

This project has been funded by Fondecyt Chile, grant Nr. 1110984. The advice of Dr. Lee Empringham and Dr. Liliana de Lillo, during the implementation of the experimental prototype used in this work, is kindly acknowledged.

Appendix

Parameters of the experimental rig

Matrix converter. Input filter $L_f = 0.625$ mH, $C_f = 2$ μF, (delta connected capacitors) $R_f = 100$ Ω, four-step commutation method implemented with a 0.7 μs for each step. Matrix converter controlled with a 12.5 kHz switching frequency.

MC output filter. Output filter implemented with 4 mH inductances and 40 uF capacitors.

Output load. The filter capacitors are connected in parallel with a resistive load. In the experimental test, the load is implemented using switchable resistor banks of 140 Ω per phase.

Permanent magnet machine. A "Control Techniques" PM machine of 8 poles, 2000 rpm, 5 kW has been used in the experimental tests related to variable speed operation.

Prime mover. The prime mover is a "*Marelli*" cage induction machine, 2 poles, 2910 rpm, 5.5 kW, 380 V. A commercial inverter is used for speed control purposes.

References

[1] Cardenas R, Pena R. Sensorless vector control of induction machines for variable-speed wind energy applications. IEEE Transactions on Energy Conversion 2004;19(1):196–205.
[2] Zinger DS, Muljadi E. Annualized wind energy improvement using variable speeds. IEEE Transactions on Industry Applications 1997;33(6):1444–7.
[3] Malik SRP, Hope GS. Real-time test results with adaptive speed controllers for a diesel prime-mover. IEEE Transactions on Energy Conversion 1992;7(2):499–505.
[4] Pena R, Cardenas R, Proboste J, Clare J, Asher G. Wind-diesel generation using doubly fed induction machines. IEEE Transactions on Energy Conversion 2008;23(1):202–14.
[5] Guerrero JM, et al. Distributed generation: toward a new energy paradigm. Industrial Electronics Magazine, IEEE 2010;4(1):52–64.
[6] Vasquez JC, Guerrero JM, Gregorio E, Rodriguez P, Teodorescu R, Blaabjerg F. Adaptive droop control applied to distributed generation inverters connected to the grid. In: ISIE 2008. IEEE international symposium on industrial electronics; 2008. p. 2420–5.
[7] Cardenas-Dobson R, Juri C, Pena R, Wheeler P, Clare J. The application of resonant controllers to 4-leg matrix converters feeding unbalanced or nonlinear loads. IEEE Transactions on Power Electronics 2011;PP(99):1.
[8] Vechiu I, Curea O, Camblong H. Transient operation of a four-leg inverter for autonomous applications with unbalanced load. IEEE Transactions on Power Electronics Feb. 2010;25(2):399–407.
[9] Li X, Deng Z, Chen Z, Fei Q. Analysis and simplification of three-dimensional space vector PWM for three-phase four-leg inverters. IEEE Transactions on Industrial Electronics Feb. 2011;58(2):450–64.

[10] Wheeler PW, Zanchetta P, Clare JC, Empringham L, Bland M, Katsis D. A utility power supply based on a four-output leg matrix converter. IEEE Transactions on Industry Applications 2008;44(1):174–86.
[11] Deng F, Chen Z. Power control of permanent magnet generator based variable speed wind turbines. In: 2009 International Conference on Electrical Machines and Systems, vol. 3; 2009. p. 1–6. no. 4.
[12] Liserre M, Member S, Cárdenas R, Molinas M, Rodríguez J. Overview of multi-MW wind turbines and wind parks. IEEE Transactions on Industrial Electronics 2011;58(4):1081–95.
[13] Ei-Barbari S, Hofmann W. Digital control of a four leg inverter for standalone photovoltaic systems with unbalanced load. no. 2. In: 26th Annual Conference of the IEEE Industrial Electronics Society. IECON 2000; 2000. p. 729–34.
[14] Cardenas-Dobson R, Pena R, Wheeler P, Clare J. Experimental validation of a space vector modulation algorithm for four-leg matrix converters. IEEE Transactions on Industrial Electronics 2011;58(4):1282–93.
[15] Wheeler PW, Rodriguez J, Clare JC, Empringham L, Weinstein A. Matrix converters: a technology review. IEEE Transactions on Industrial Electronics Apr. 2002;49(2):276–88.
[16] Podlesak TF, Katsis DC, Wheeler PW, Clare JC, Empringham L, Bland M. A 150-kVA vector-controlled matrix converter induction motor drive. IEEE Transactions on Industry Applications May. 2005;41(3):841–7.
[17] Wheeler PW, Clare JC, Empringham L, Bland M, Kerris KG. Matrix converters. IEEE Industry Applications Magazine Jan. 2004;10(1):59–65.
[18] Arap D. Modelling, simulation, and performance analysis of a hybrid power system for mobile medical clinic. Kassel: Ph.D thesis. University of Kassel Germany; 2004.
[19] Cardenas R, Pena R, Tobar G, Clare J, Wheeler P, Asher G. Stability analysis of a wind energy conversion system based on a doubly fed induction generator fed by a matrix converter. IEEE Transactions on Industrial Electronics Oct. 2009;56(10):4194–206.
[20] Cardenas R, Pena R, Wheeler P, Clare J. "Resonant controllers for 4-leg matrix converters. In: 2010 IEEE international symposium on industrial electronics; 2010. p. 1027–32.
[21] Ng CH, Ran L, Bumby J. Unbalanced-grid-fault ride-through control for a wind turbine inverter. IEEE Transactions on Industry Applications 2008;44(3):845–56.
[22] Pena R, Cardenas R, Escobar E, Clare J, Wheeler P. Control system for unbalanced operation of stand-alone doubly fed induction generator. IEEE Transactions on Energy Conversion 2007;22(2):544–5.
[23] Fortescue C. Method of symmetrical coordinates applied to the solution of polyphase networks. AIEE Transactions 1918;37(2):1027–140.
[24] Timbus A, Liserre M, Teodorescu R, Rodriguez P, Blaabjerg F. Evaluation of current controllers for distributed power generation systems. IEEE Transactions on Power Electronics Power 2009;24(3):654–64.
[25] Buso B, Mattavelli P. In: Hudgins J, editor. Digital control in power electronics. Morgan and Claypool; 2006.
[26] Zmood DN, Holmes DG. Stationary frame current regulation of PWM inverters with zero steady-state error. IEEE Transactions on Power Electronics May 2003;18(3):814–22.
[27] Zmood DN, Holmes DG. Improved voltage regulation for current-source inverters. IEEE Transactions on Industry Applications 2001;37(4):1028–36.
[28] Hwang JWG, Winkelnkemper M, Lehn PW. "Design of an optimal stationary frame controller for grid connected AC–DC converters. In: IEEE Industrial Electronics, IECON 2006-32nd Annual Conference; 2006. p. 167–72.
[29] Hwang JG, Lehn PW, Winkelnkemper M. A generalized class of stationary frame-current controllers for grid-connected AC-DC converters. IEEE Transactions on Power Delivery 2010;25(4):2742–51.
[30] Zmood DN, Holmes DG. "Stationary frame current regulation of PWM inverters with zero steady state error. In: 30th Annual IEEE Power Electronics Specialists Conference, vol. 2; 1999. p. 1185–90.
[31] Teodorescu R, Blaabjerg F, Liserre M, Loh PC. Proportional-resonant controllers and filters for grid-connected voltage-source converters. Electric Power Applications, IEE Proceedings 2006;153(5):750–62.
[32] Roy S, Malik OP, Hope GS. A k-step predictive scheme for speed control of diesel driven power plants. IEEE Transactions on Industry Applications 1993;29(2):389–96.